



Strong Southern African Monsoon and weak Mozambique Channel throughflow during Heinrich events: Implication for Agulhas leakage

Yue Ma^a, Syee Weldeab^{a,*}, Ralph R. Schneider^b, Nils Andersen^c, Dieter Garbe-Schönberg^b, Tobias Friedrich^d

^a Department of Earth Science, University of California, Santa Barbara, CA, USA

^b Institute of Geosciences, Kiel University, Kiel, Germany

^c Leibniz Laboratory for Radiometric Dating and Stable Isotope Research, Kiel University, Kiel, Germany

^d Department of Oceanography, School of Ocean & Earth Science and Technology, University of Hawai'i at Mānoa, HI, USA

ARTICLE INFO

Article history:

Received 6 March 2021

Received in revised form 31 July 2021

Accepted 4 August 2021

Available online xxxx

Editor: Y. Asmerom

Keywords:

Southern African Monsoon

Heinrich stadials

Mozambique Channel throughflow

Agulhas leakage

ABSTRACT

The Mozambique Channel is a conduit of trade wind-driven throughflow that is a key component of the Agulhas Current and Agulhas leakage, a flux of warm and salty water from the tropical Indo-Pacific to the Atlantic Ocean. Agulhas leakage is thought to modulate Atlantic meridional overturning circulation variability. Previous studies from the Cape Basin suggest that enhanced Agulhas leakage played an important role in accelerating glacial terminations. The southern African monsoon response to abrupt climate changes associated with meltwater-induced reorganizations of the North Atlantic meridional overturning circulation, and its impact on the Mozambique Channel throughflow and, by extension, on the Agulhas leakage is not well understood. Here we present a high-resolution 26,000 year-long hydroclimate record of northern Madagascar, a core region of the southern hemisphere monsoon domain, and a mixed layer temperature reconstruction using sediment cores collected from the runoff-influenced eastern Mozambique Channel. The record indicates precipitation increases centered at 11.7–12.5 thousand years before present (kyr BP), 14.5–19 kyr BP, 23–24 kyr BP, 25–26 kyr BP. Considering age model uncertainties, this is the first strong evidence for southern African monsoon strengthening in response to meltwater-induced northern high latitude climate instabilities during the Younger Dryas (YD), Heinrich Stadial 1 (HS1), HS2 and the HS-like event prior to HS2, in agreement with the results of transient climate simulations. Furthermore, our study shows a reversal of the mixed layer temperature gradient between the western and eastern Mozambique Channel during Heinrich event 1 (HE1). We posit that the gradient reversal indicates a weakening of the trade wind-driven South Equatorial Current and Mozambique Channel throughflow that likely weakened the Agulhas leakage, potentially creating a feedback that may have contributed to the sustained weakening of the AMOC during HE1 by reducing the amount of heat and salt leakage into the Atlantic.

© 2021 The Author(s). Published by Elsevier B.V. This is an open access article under the CC BY license (<http://creativecommons.org/licenses/by/4.0/>).

1. Introduction

Oceanic gateways play a key role in interbasinal heat and salt exchanges, modulating global ocean circulation and hydrological cycles (Biaostoch et al., 2015). The Mozambique Channel is one of the two pathways through which warm and salty tropical Indo-Pacific Ocean water is funneled to the southwestern Indian Ocean to form the Agulhas Current and Agulhas Return Current (Beal and Elipot, 2016; Biaostoch et al., 2015). To the south of the tip of South Africa, a small fraction of tropical Indo-Pacific Ocean water leaks

(Agulhas leakage) into the Atlantic Ocean in the form of mesoscale eddies (Beal and Elipot, 2016; Biaostoch et al., 2015). Recent observations suggest that over the last five decades the Agulhas Current has broadened and Agulhas leakage is increasing in response to a warming climate (Beal and Elipot, 2016; Biaostoch et al., 2015). Instrumental and simulation data show that a southward shift of maximum latitude of the Southern Hemisphere westerlies and an intensification of the monsoon wind fields over the tropical Indian Ocean strengthen the Agulhas Current and the associated Agulhas leakage (Backeberg et al., 2012; Beal and Elipot, 2016; Biaostoch et al., 2015). A sustained increase of leakage of salty water into the South Atlantic and its advection to the North Atlantic is thought to stabilize and strengthen the Atlantic Meridional Overturning Circulation (AMOC) (Backeberg et al., 2012; Biaostoch et al., 2015).

* Corresponding author.

E-mail address: sweldeab@ucsb.edu (S. Weldeab).

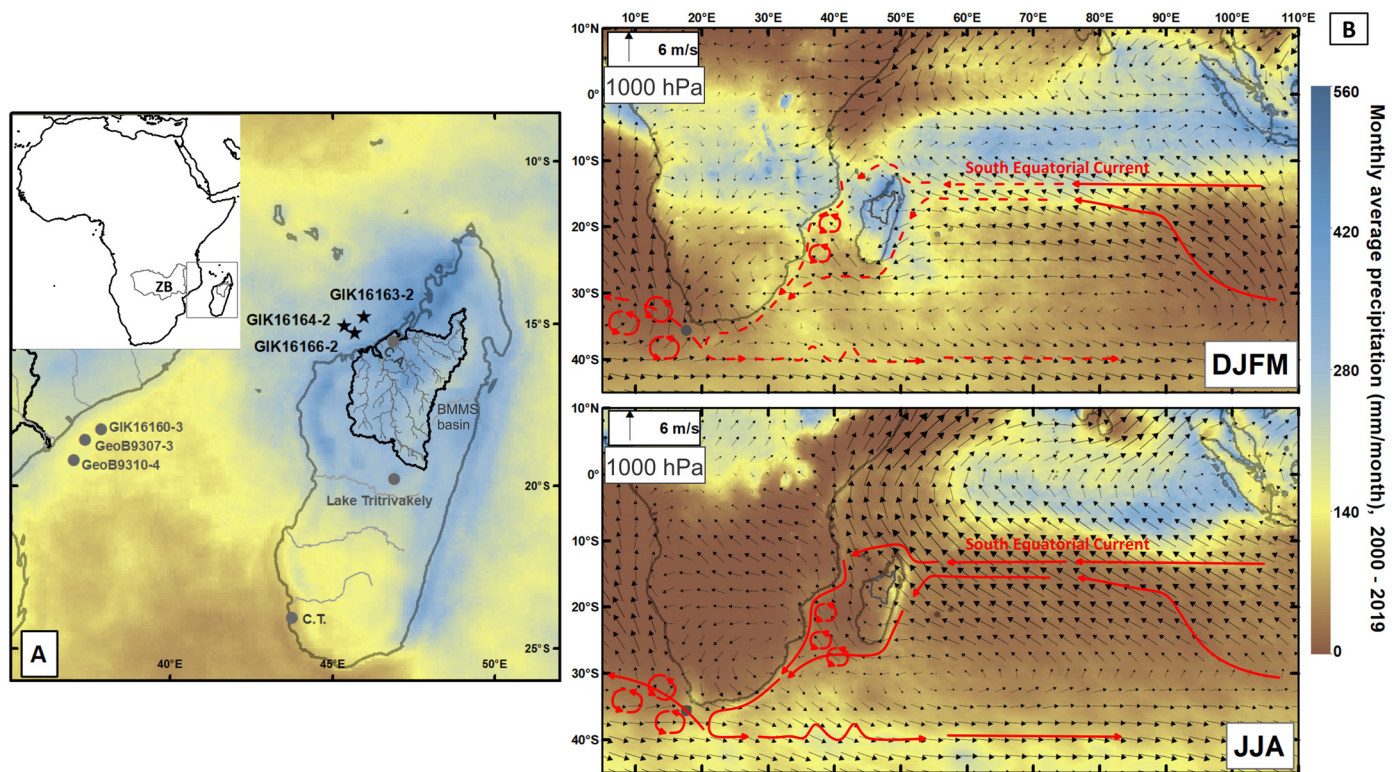


Fig. 1. Summer and winter precipitation over the tropical Indian Ocean and adjacent land mass and wind-driven ocean surface currents. A) A close-up view of the study area, showing austral summer precipitation (December-to-March) and sampling location of marine sediment cores GIK16163-2, GIK16164-2, and GIK16166-2 that are used in this study. Also indicated is the boundary of the Betsiboka, Mahavavy, Mahajamba, and Sofia (BMMS) basin and sites of previous studies with which our result is compared (CA: Cave Anjohibe and Anjokipoty; CT: Cave Tsimanampesotse). Location and extent of Zambezi Basin (ZB) is indicated in the insert. B) Seasonal precipitation and wind field patterns over the tropical Indian Ocean and adjacent land mass during austral summer (December-to-March: DJFM) and austral winter (June-to-August: JJA). Monthly average precipitation and surface winds collected over the time window between 2000 and 2019 (Huffman et al., 2019; Kalnay et al., 1996). Red arrows indicate a schematic depiction of relevant ocean surface currents, emphasizing the role of Indian Ocean gyre (Ridderinkhof et al., 2010; Hutchinson et al., 2018). Dotted lines in Fig. 1B (top) indicate weaker currents compared to those indicated in Fig. 1B (bottom). The gray dot ($35^{\circ}35\text{ S}/17^{\circ}41\text{ E}$) in the Cape Basin indicates the core location studied by Peeters et al. (2004). (For interpretation of the colors in the figure(s), the reader is referred to the web version of this article.)

On orbital scales, paleoclimate studies suggest increases of the Agulhas leakage during deglaciations and hypothesize that these increases were associated with a southward shift of the westerlies and contributed to strengthening of the AMOC and, as a result, accelerated the termination of the glacial episodes (Caley et al., 2012; Marino et al., 2013; Peeters et al., 2004; Simon et al., 2013). Most of these studies are based on marine sediments from the southwestern sector of the Indian Ocean and assume a direct link between changes in the strength of the Agulhas Current and Agulhas leakage (Caley et al., 2012; Marino et al., 2013; Simon et al., 2013). An exception is the study by Peeters et al. (2004) at a site that is located in the Atlantic sector of the Agulhas leakage pathway and most likely records faunal signatures linked to changes in the Agulhas leakage (Fig. 1). The relatively low resolution of the existing records, however, does not allow detailed examinations of the response of the Agulhas leakage to millennial-scale climate perturbations such as the Heinrich events. Furthermore, past changes in the water mass transport through the Mozambique Channel and their potential association with changes in trade winds have not been considered, despite being critical for an improved understanding of tropical influence on the Agulhas leakage (Backeberg et al., 2012). In particular, the response of the southern African monsoon to meltwater-induced northern high latitude climate instabilities and the impact on the monsoonal wind-driven water mass transport through the Mozambique Channel have not yet been explored. The limited number of paleoclimate studies focusing on the southern African monsoon draw a complex and spatially heterogeneous pattern (Khon et al., 2014; Schefuß et al., 2011; Scroton et al., 2019; Wang et al., 2013a,b; Weldeab et al., 2014; Williamson et

al., 1998), most likely reflecting regionally heterogeneous response and varying proxy sensitivity. The lack of spatially and temporally coherent hydroclimate records of the region impedes efforts to deduce the dominant forcings and their role in co-shaping global climate changes.

The results of this study show for the first time strong and consistent evidence of southern African monsoon strengthening during meltwater-induced, large-scale atmospheric perturbations during the last deglacial and the last glacial. Based on surface temperature gradient reconstruction within the Mozambique Channel and results of climate simulation, we infer a weaker water mass transport through the channel during the early part of the deglaciation, potentially reducing the tropical Indian Ocean's influence on the Agulhas leakage.

2. Regional setting

2.1. Precipitation over Madagascar

Precipitation over Madagascar is primarily controlled by the southern African monsoon which is a component of the Southern Hemisphere monsoon system (Fig. 1). During austral summer (December-to-March: DJFM), the Inter-Tropical Convergence Zone (ITCZ) shifts southward and brings monsoon rainfall to northwestern Madagascar (Fig. 1). Over the Betsiboka, Mahavavy, Mahajamba, and Sofia (BMMS) Basin, which is the focus of this study (Figs. 1A, 2A-D), DJFM precipitation varies between 250 and 560 mm/month (Fig. 2B). The low elevation region ($< 700\text{ m}$ above sea level) within the BMMS Basin receives more precipitation (300-

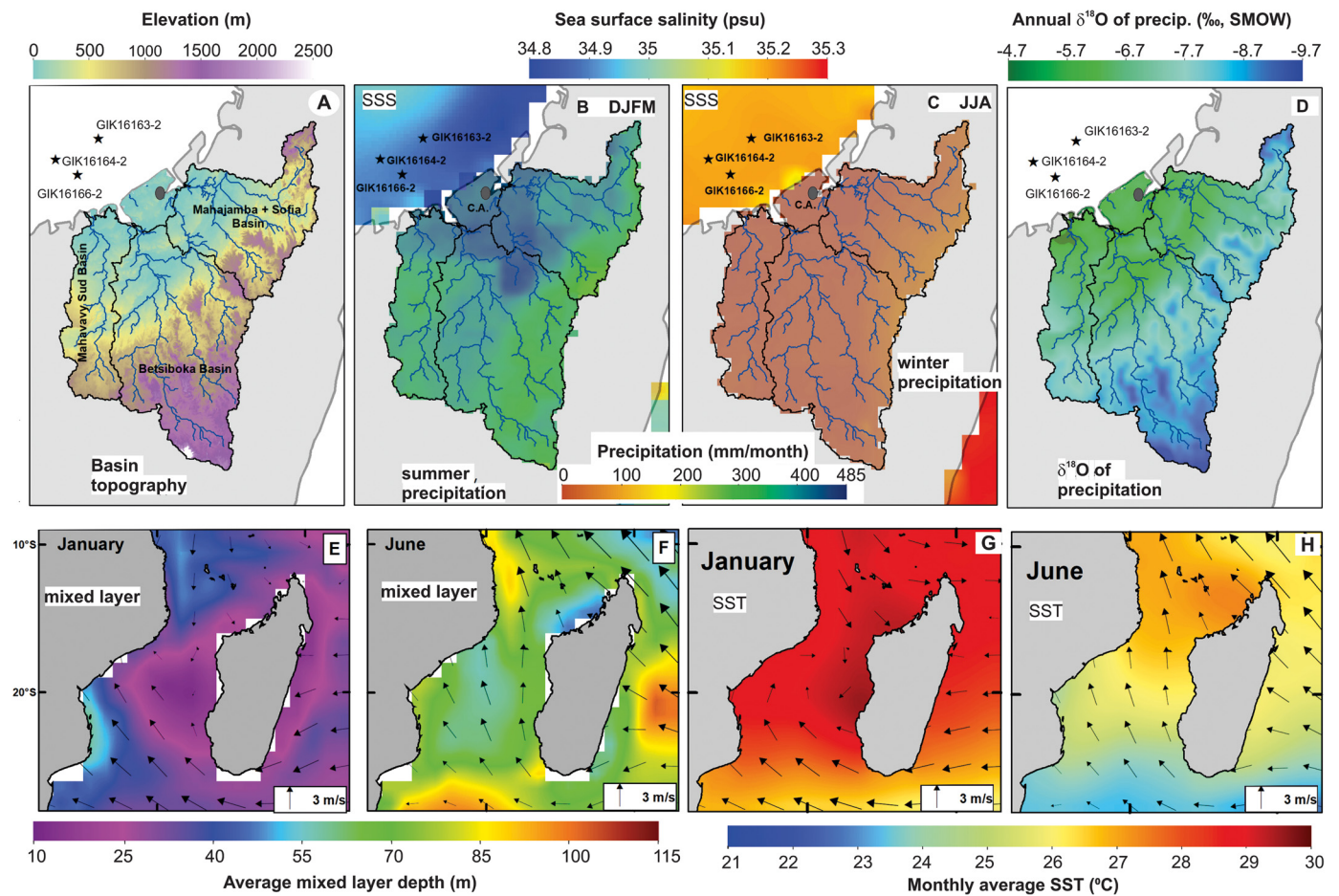


Fig. 2. Hydroclimatic and topographic features of the BMMS basin and its runoff impact on the sea surface salinity (SSS) of the northeastern Mozambique Channel. A) Topography of the BMMS basin U.S. Geological Survey's Center for Earth Resources Observation and Science (1996). B) and C) Monthly average precipitation (2000 to 2019) during wet and dry season over Madagascar (Huffman et al., 2019). Shown is also runoff impact on the SSS over the sediment core locations (Wentz et al., 2014). D) Spatial patterns of annually averaged and spatially interpolated $\delta^{18}\text{O}$ of precipitation (Bowen and Revenaugh, 2003). E and F) Mixed layer depth and monthly surface winds in January and June (Behringer and Xue, 2004; Kalnay et al., 1996). G and H) Monthly averaged (2000–2019) sea surface temperature (SST) and direction and strength of wind indicated by arrows for January (G) and June (H) (Behringer and Xue, 2004; Kalnay et al., 1996).

560 mm/month) compared to the high elevation (> 1000 m above sea level), which receives 250 to 300 mm/month precipitation during the wet season (Figs. 1B and 2B). During austral winter (June to August: JJA), northwestern Madagascar receives monthly precipitation of less than 20 mm/month (Figs. 1B and 2C). Relatively low-resolution data of annually averaged $\delta^{18}\text{O}$ of precipitation over the BMMS river basin show a strong modulation by the topography (Bowen and Revenaugh, 2003), with $\delta^{18}\text{O}$ values between -4.82‰ and -5.74‰ over the low elevation (< 700 m above sea level) and -9.4‰ and -7.6‰ over the high elevation region (> 1000 m above sea level) (Figs. 2A, D). With a combined catchment area of 116,000 km², the BMMS basin drains northwestern Madagascar (Figs. 1 and 2). River discharge records are available only for four tributaries that drain high elevation and relatively dry areas of 41,000 km² (35% of the BMMS basin size) with an annual discharge volume of 36 km³ (Fig. S2). The seasonal runoff from the BMMS rivers has noticeable impact on the sea surface salinity (SSS) of the northeastern part of the Mozambique Channel (Figs. 2B and 2C). The preservation of the runoff imprint in the surface water of northeastern Mozambique Channel is enhanced due to an orographically weakened wind field and surface current mixing, resulting in a relatively shallow mixed layer (Figs. 2E & F).

2.2. Mozambique Channel

2.2.1. Seasonal SST pattern

Sea surface temperature within the Mozambique Channel varies seasonally and spatially (Figs. 2G–H). Average surface water temperatures are 29–30°C and 26–27°C during the austral summer and winter, respectively, and surface water in the eastern part of the Mozambique Channel is warmer than in the western part (Figs. 2G–H, Fig. S1). The resulting east-west temperature gradient is about 1.2°C in the north (at 15°S) and weakens to 0.9°C in the south (at 24°S). Spatial SST variation in the Mozambique Channel occurs due to spatially varying wind fields and a southward propagating current and eddies along the western part of the channel (Swart et al., 2010). The mountains in eastern Madagascar significantly weaken and divert the easterly winds (Figs. 2G–H, Fig. S1), leading to a shallower mixed layer depth in the eastern Mozambique Channel (Figs. 2E–F) and, as a result, elevated SST compared to the western Mozambique Channel. The southward passage of eddies and currents also contributes to the east-west SST gradient. On the west side of the Mozambique Channel, anticyclonic eddies cause a strong tilt of the thermal structure of the upper water column (Swart et al., 2010). For instance, during a passage of an anticyclonic eddy, Swart et al. (2010) observed that on the western Mozambique Channel (west of ~36°E) the 20°C isotherm was 30–40 m below the sea surface (Swart et al., 2010). In contrast, in the central and eastern Mozambique Channel (east of ~38°E),

the 20 °C isotherm was approximately 200 m below the sea surface. As a consequence, the mixed layer in the western part of Mozambique Channel is subjected to a stronger mixing with cold water at shallower depth than in the central and western part of the Mozambique Channel. Though spatially limited, cyclonic eddies develop along the African continental margin and bring relatively cold deep water to the mixed layer, leading to anomalous surface water cooling of 2–4 °C during the austral summer (Malauene et al., 2014). Interannual variability of generation and passage of cyclonic and anticyclonic eddies leaves a noticeable thermal imprint on the mixed layer water of Mozambique Channel and its east-west gradients (Malauene et al., 2014; Ridderinkhof et al., 2010).

2.2.2. Mozambique Channel: a conduit for warm and saline water mass transport

The Mozambique Channel is a conduit for the wind-driven South Equatorial Current and anticyclonic and cyclonic eddies that develop north of the Mozambique Channel and propagate along the western boundary (Backeberg et al., 2012; Swart et al., 2010). The anticyclonic eddies carry, on average, a warm and salty water mass of 16.7 ± 3.1 Sv: 10^6 m³/s) and feed the Agulhas Current (Backeberg et al., 2012; Ridderinkhof et al., 2010; Swart et al., 2010). Seasonal wind fields over the tropical Indian Ocean and associated Ekman transport exert a strong control on the amount of water mass transport through the Mozambique Channel and east of Madagascar (Backeberg et al., 2012). During austral summer, the Indian Ocean monsoon and the weakening of southeast winds result in a weak Southern Equatorial Current and Ekman transport both east and west of Madagascar (Fig. 1B). During austral winter, the strengthening and continuous southeast winds generate a strong Ekman transport and increase the amount of water mass transport through the Channel (Fig. 1B). Water mass transport through the Mozambique Channel shows a strong interannual variability (8.9 Sv) that is thought to be linked to the developments of Indian Ocean Dipole (IOD), with positive IODs weakening the South Equatorial Current and Mozambique Channel throughflow (Ridderinkhof et al., 2010). As the Mozambique Channel throughflow joins the Southeast Madagascar Current (Fig. 1B), they together form the Agulhas Current (Swart et al., 2010). Occasionally, the Agulhas Current sheds eddies that leak (Agulhas Leakage) into the Atlantic Ocean. The warm and salty Agulhas leakages advect to the North Atlantic and are thought to influence the decadal variability of AMOC (Backeberg et al., 2012; Biastoch et al., 2015; Swart et al., 2010).

3. Materials and methods

This study focuses on three marine sediment cores that were collected during the Meteor Cruise M75 in 2008 (GIK16163-2: 14°45.47'S, 45°59.20'E, water depth 2579 m; GIK16164-2: 15°30.66'S, 45°22.46'E, water depth 2915 m; and GIK16166-2: 15°16.27'S, 45°41.43'E, water depth 2099 m) (Fig. 1A). To establish an age model for each core, a total of 31 radiocarbon analyses were carried out on tests of mixed-layer dwelling planktonic foraminifers at the Leibniz Laboratory for Radiometric Dating and Stable Isotope Research (Kiel University Kiel, Germany) (Table S1). The final age model used in this study is based on the Bacon software (Blaauw and Christen, 2011). We analyzed Mg/Ca and $\delta^{18}\text{O}$ in *Globigerinoides ruber* white and established Mg/Ca-based mixed layer temperature estimates and $\delta^{18}\text{O}$ of mixed layer. A detailed description of all methods, measurements, age model, and error analyses is provided in the supplemental information.

4. Results

4.1. Sediment accumulation rate

The sedimentation rate in all three cores shows temporal and spatial variation (Fig. 3), with the glacial and deglacial interval showing relatively high sedimentation rates (5–35 cm/kyr) relative to the Holocene (2–5 cm/kyr). Site GIK16166-2, which is more proximal to the river mouth, displays the highest sedimentation rate followed by GIK16163-2 (Fig. 3). Common to both cores is an interval of an exceptionally high sedimentation rate centered between 15.5 and 13 kyr BP (37 cm/kyr in GIK16166-2 and 10 cm/kyr in GIK16163-2). Reconstruction of the sea level related changes in the distance between the river mouths and core sites suggests that changes in sedimentation rate at each core site remained largely independent of distance from the river mouth throughout the glacial, deglacial, and late Holocene. This suggests that changes in sedimentation rate are likely associated with changes in sediment discharge from the catchments linked with variable precipitation and erosion in the river basins (Figs. 3 and S4). Only sedimentation rate changes between 6 and 9 kyr BP coincide with changes in river mouth to core site distance.

4.2. Oxygen isotope composition ($\delta^{18}\text{O}$) and Mg/Ca-based temperature estimates

The $\delta^{18}\text{O}$ time-series of *G. ruber* ($\delta^{18}\text{O}_{G. ruber}$) (Figs. 4A, A', A''), a composite imprint of calcification temperature, global ice volume and local $\delta^{18}\text{O}$ seawater changes, shows a very similar pattern in all three cores, with relatively high (0.5‰ to -1‰) and relatively low values (-2 to -2.5‰) during the glacial and Holocene, respectively, bridged by a gradual decrease during the deglaciation and the early Holocene (17–9 kyr BP). Superimposed on the gradual deglacial change, a relatively abrupt decline in $\delta^{18}\text{O}_{G. ruber}$ is evident during Younger Dryas (YD) in all three cores, although the magnitude and timing of changes varies between the cores, most likely due to a difference in river mouth to core site distance and age model uncertainties, respectively.

The Mg/Ca data show an increasing trend from about 3.25 $\mu\text{mol/mol}$ during the glacial period to about 4.25 $\mu\text{mol/mol}$ during the Holocene (Fig. 4B). The individual record shows high frequency variability, some of which are present in all cores. In some segments, the resolution of Mg/Ca time-series is lower than the $\delta^{18}\text{O}_{G. ruber}$ record due to low foraminifer abundance, sample loss during cleaning, and removal of data points with elevated silicate phases, as indicated by high Al/Ca values. Because the core sites are closely located to each other, we assume that the spatial difference of mixed layer temperature, if any, in the past was significantly smaller than the uncertainty of SST reconstruction (± 0.65 °C). Hence, using the Mg/Ca data of all three cores and a bin window of 200 years, we create a single high-resolution temperature record. The composite record indicates a last glacial (25–19 kyr BP) mixed layer temperature that varies, on average, between 23 and 24 °C (Fig. 4D). Starting at 18 kyr BP, the temperature increases gradually, reaching a maximum value of 27 °C at 6 kyr BP. Between the mid and late Holocene, mixed layer temperature shows a decrease by about 1 °C (Fig. 4D).

As described in the Methods section and supplementary information, we removed the ice volume and calcification temperature effects from the $\delta^{18}\text{O}_{G. ruber}$ time-series and obtained an estimate of the $\delta^{18}\text{O}$ of local mixed layer sea water ($\delta^{18}\text{O}_{\text{SW}}$) (Fig. 4E). A common feature to all three cores is that on orbital scale the records show low $\delta^{18}\text{O}_{\text{SW}}$ values (-0.6‰ to -0.4‰) during the glacial, increasing $\delta^{18}\text{O}_{\text{SW}}$ values during the deglacial, reaching their highest values (0‰ to 0.4‰) at about 13–14 kyr BP. During the Holocene the $\delta^{18}\text{O}_{\text{SW}}$ reaches values that vary between 0.2‰

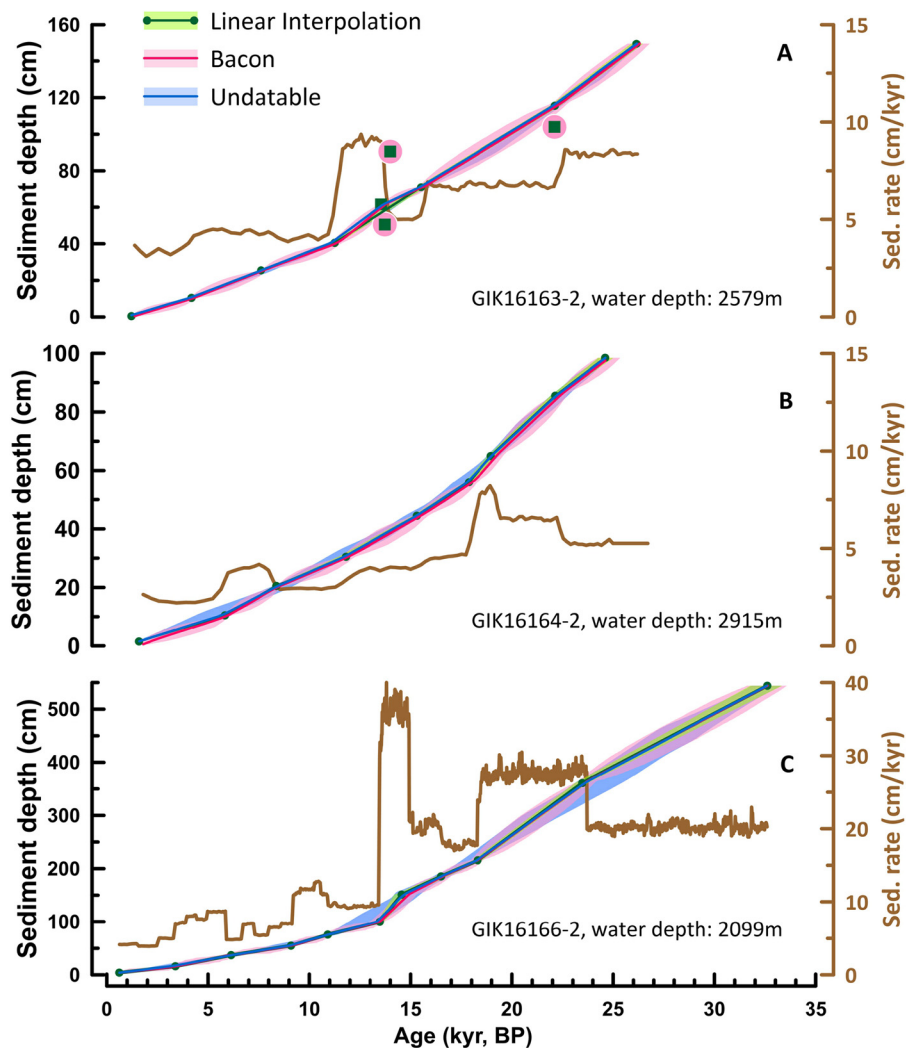


Fig. 3. Age models and sedimentation rates of marine sediment cores used in this study: A) GIK16163-2, B) GIK16164-2, and C) GIK 16166-2. Green blue, and red lines indicate age models based on linear interpolation, based on the Bacon software (Blaauw and Christen, 2011), and the Undatable software (Lougheed and Obrochta, 2019), respectively. The envelopes indicate 2σ error estimates. Data points indicated by green squares and pink circles were excluded from the linear interpolation and Bacon age models, respectively. The final age model used in this study is based on the Bacon software (Blaauw and Christen, 2011). Shown is also sediment accumulation rate calculated using the results of the Bacon age models.

and -0.4‰ . Superimposed on the orbital scale trend, the $\delta^{18}\text{O}_{\text{SW}}$ records reveal multi-centennial scale oscillations. The most prominent of these features are centered between 4 and 1 kyr BP, 13 and 11 kyr BP, 19 and 14 kyr BP, and 26 and 23 kyr BP (Fig. 4E) and have relatively low $\delta^{18}\text{O}_{\text{SW}}$ values.

5. Discussion

5.1. Regional hydroclimate

Our interpretation of the local $\delta^{18}\text{O}_{\text{SW}}$ record is that changes in $\delta^{18}\text{O}_{\text{SW}}$ reflect changes in the amount of precipitation and isotope composition of precipitation over the river basin. Isotope composition changes in precipitation can occur as a result of changes in seasonality and changes in the moisture source. These changes can amplify or weaken the isotope signatures related to changes in the rainfall amount. We hypothesize that change in the amount of precipitation is the dominant factor that shapes the $\delta^{18}\text{O}$ of the mixed layer of the study area. This hypothesis is in part supported by an elevated sedimentation rate during episodes of low $\delta^{18}\text{O}_{\text{SW}}$ value, indicating increased runoff and riverine sediment loads (Fig. S4). As shown and discussed below, an independent hydroclimate reconstruction from the southern periphery of the BMMS basin

and the results of climate simulation substantiate our hypothesis. Hence, our $\delta^{18}\text{O}_{\text{SW}}$ record provides insights into past hydroclimate changes. To assess the effect of the Holocene-to-glacial sea level change on the distance between the core sites and the resultant effects on the runoff signal at each core site, we create a sea level-dependent distance profile between the river mouth and core site (Fig. S3). The largest changes in sediment accumulation rates and riverine isotope imprint occurred at the time when the distance between the river mouth and core site was not changing (Figs. 3 and 4).

5.1.1. Orbital scale changes in hydroclimate

According to the above hypothesis, the relatively low $\delta^{18}\text{O}_{\text{SW}}$ values during the last glacial period, recorded in all three sediment cores, indicate a relatively humid period over northwestern Madagascar as low $\delta^{18}\text{O}$ of freshwater runoff freshens the sea surface water over the core sites. At the orbital time scales, these data imply that the humid glacial episode is followed by a general drying trend across the deglaciation (Figs. 4A and 5A). The Holocene varied between dry and moderately humid conditions. The regional context of the orbital scale trend will be discussed in section 5.1.4.

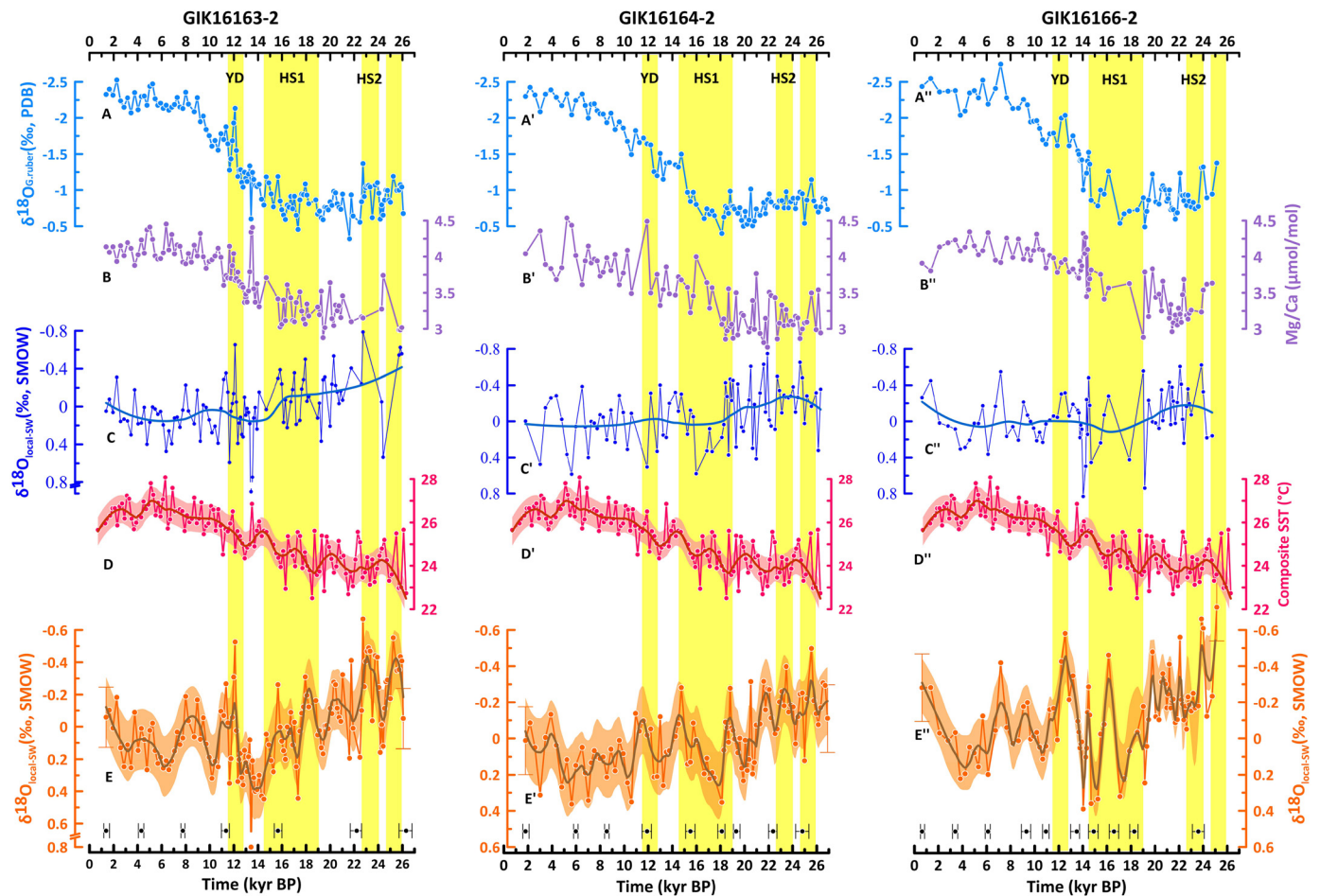


Fig. 4. Climate proxy parameters analyzed in the three marine sediment cores. A and B) $\delta^{18}\text{O}_{G.ruber}$ and Mg/Ca time-series analyzed in test of *G. ruber*. C) local $\delta^{18}\text{O}_{SW}$ obtained by correcting the $\delta^{18}\text{O}_{G.ruber}$ for temperature and ice volume effects. For the correction of temperature effect, temperature reconstruction based on the Mg/Ca data shown in Fig. B was used. D) Mg/Ca-based mixed layer temperature estimated using a binned (with a 200-year bin window) composite of Mg/Ca data of all three cores, as shown in B. The thick line and envelope indicate a LOESS fit and its 1σ uncertainty. E) local $\delta^{18}\text{O}_{SW}$ obtained by correcting the $\delta^{18}\text{O}_{G.ruber}$ for temperature and ice volume effects. For the correction of temperature effect, the composite temperature record (Fig. 4D) was used. Black symbols and horizontal balks along the x-axes show age model control points and age model 2σ uncertainty. Yellow shaded areas indicate episodes of meltwater-induced perturbations of atmospheric and ocean circulation.

5.1.2. Millennial scale southern African monsoon strengthening and its link to northern high latitude climate changes

On the millennial scale, the $\delta^{18}\text{O}_{SW}$ time-series of all three cores exhibit several episodes that are marked by relatively low $\delta^{18}\text{O}_{SW}$ values, indicating relatively wet phases. We note that the timing and duration of these episodes varies slightly between the three cores due to age model uncertainties and varying resolution. In the following discussion, we will mainly focus on the $\delta^{18}\text{O}_{SW}$ record of GIK16163-2 because this core covers a longer record, is more highly resolved, and has generally a stronger $\delta^{18}\text{O}_{SW}$ signature than the other two cores (Figs. 4 and 5). In GIK16163-2, the $\delta^{18}\text{O}_{SW}$ record indicates several episodes of relatively wet conditions including during the late Holocene (1-5 kyr BP) (Fig. 4E), the mid-to-early Holocene (9.7-7.2 kyr BP) and early Holocene (11.5-10.9 kyr BP). The most prominent features and the main focus of our discussion are centered at 12.5-11.7 kyr BP, 19-14.5 kyr BP, 24-22.7 and 26-24.7 kyr BP. Considering age model uncertainties up to ± 500 years, the timing of the prominent wet phases in northwestern Madagascar coincides with the timing of the YD, Heinrich Stadial 1 (HS1), HS2, and a HS-like event that occurred prior to HS2 (Fig. 5).

HS-like event and HS2: At Site GIK16163-2 the HS-like event is centered at 25.5 kyr BP (26-24.7 kyr BP) and characterized by a $\delta^{18}\text{O}_{SW}$ decline of 0.4-0.5‰ relative to the time intervals prior and after the event, indicating an episode of southern African monsoon

strengthening (Fig. 5A). This climate event is identified as layer “d” in North Atlantic sediments that show enhanced deposition of ice rafted lithics (Fig. 5B) (Bond et al., 1997). HS2 occurred between 22.7 and 24 kyr BP and is marked by a $\delta^{18}\text{O}_{SW}$ drop of 0.6‰ relative to the background levels. Similar to HS2, the timing of the HS-like event is coincident, within the uncertainty of age models, with a weakening of AMOC (Lippold et al., 2009), air cooling over Greenland (Alley, 2000) (Fig. 5E), and a drop of North Atlantic sea surface temperature (Martrat et al., 2007). It is also recognized in Greenland ice cores as an interval with a substantial increase of dust accumulation (Simonsen et al., 2019) and elevated concentration of Ca^{2+} (Mayewski et al., 1997), a proxy for Asian dust input and a common feature of most Heinrich stadials, including HS2 (Figs. 5C and D). In the tropics, similar to HS2, the HS-like event is recorded as an interval of weak Northern Hemisphere monsoon systems (Cheng et al., 2012; Weldeab, 2012; Weldeab et al., 2007) and a strengthening of the South American monsoon (Novello et al., 2017), respectively, as discussed more in detail further below.

HS1: The $\delta^{18}\text{O}_{SW}$ trend and magnitude of changes that occurred within the HS1 interval show that HS1 is divided into two phases (Fig. 5A). Between 19.4 to 17.8 kyr BP the $\delta^{18}\text{O}_{SW}$ declined by 0.5‰. The early phase (19-17.5 kyr BP) of the southern African monsoon strengthening occurred within the early phase of HS1 (Phase I), as defined by Stanford et al. (2011), and coincided with the onset of AMOC weakening (McManus et al., 2004). The $\delta^{18}\text{O}_{SW}$

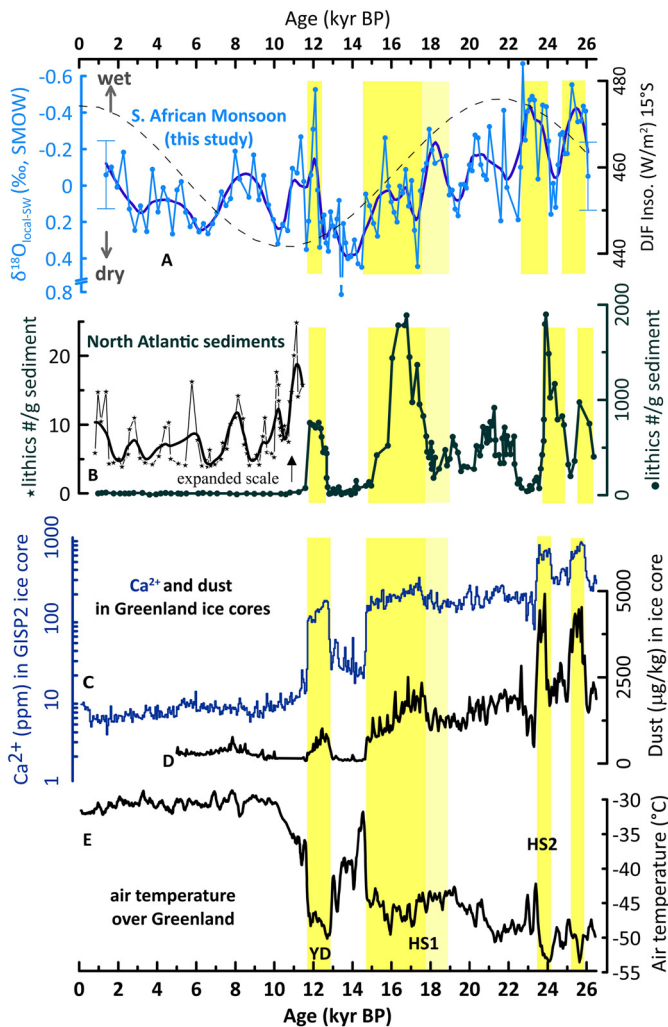


Fig. 5. Changes in the African sector of the Southern Hemisphere monsoon system and their potential link to northern high latitude climate changes. A) $\delta^{18}\text{O}_{\text{SW}}$ record reconstructed from GIK16163-2 sediment core materials and used as a proxy for hydroclimate changes over northwestern Madagascar (this study). Dashed line indicates solar insolation at 15°S during austral summer (December, January & February, DJF) (Laskar et al., 2004). B) Lithic (63–150 μm) counts per gram sediment in a North Atlantic sediment core (Bond et al., 1997). The Holocene segment of the lithic record is expanded with the thick line showing a fitting curve using LOESS function. C) Ca^{2+} concentration (ppm) analyzed (50 year mean) in GISP2 (Greenland) ice core (Mayewski et al., 1997) plotted using the GICC05 model time scale. D) Dust concentration ($\mu\text{g}/\text{kg}$, size range: 1.25–10.5 μm) analyzed in Greenland ice core (RECAP) (Simonsen et al., 2019). Air temperature estimates over Greenland based on $\delta^{18}\text{O}_{\text{ice}}$ time-series analyzed in GISP2 ice core (Alley, 2000), respectively.

record of the early phase suggests humid conditions similar to the second phase (~ 17.5 – 14.5 kyr BP) (Fig. 5A). Considering age model uncertainties, the second phase of southern African monsoon strengthening during HS1 falls within the timing of Heinrich Event 1 (HE1), as defined by Heinrich Layer 1 (Figs. 5A and B) (Stanford et al., 2011), with a substantially enhanced deposition of dust and Ca^{2+} in Greenland ice cores (Mayewski et al., 1997; Simonsen et al., 2019) (Figs. 5C and D). Compared to the HS2 and YD (see below), the hydroclimate imprint of HS1 is weaker.

Younger Dryas: One of the outstanding features of our record is an abrupt $\delta^{18}\text{O}_{\text{SW}}$ decrease by about 0.9‰ between 12.6 and 11.7 kyr BP, indicating an interval of southern African monsoon intensification (Fig. 5A). Considering an age model uncertainty of up to ± 500 years, this humid episode over northwestern Madagascar coincides with the timing of the YD (11.6–12.9 kyr BP) (Fig. 5A). As shown in Figs. 5A–E, the humid phase of northwestern Mad-

agascar is paralleled by a substantially enhanced deposition of dust and Ca^{2+} in Greenland ice cores and lithics in North Atlantic deep-sea sediments, and northern high latitude cooling (Mayewski et al., 1997; Simonsen et al., 2019). An increase of $\delta^{18}\text{O}_{\text{SW}}$ by $\sim 0.9\text{‰}$ at 11.6 kyr BP, indicating a brief spell of dry conditions, separates the YD wet episode from the early Holocene wet interval centered between 11.5 and 10.9 kyr BP (Fig. 5A). Noting the brief duration of the event and age model uncertainties, the wet period (11.5–10.9 kyr BP) is matched by an elevated amount of lithics in North Atlantic sediments, though at low concentration compared to the lithics deposition during glacial and deglaciation (Fig. 5B).

Taken together, the deposition of ice rafted debris and lithics in the North Atlantic during the glacial and deglacial are indicative of episodes of enhanced meltwater discharge whose effect is manifested in North Atlantic surface freshening, AMOC weakening, and, as a result, North Atlantic sea surface temperature and air temperature drop (Alley, 2000; Martrat et al., 2007; McManus et al., 2004). Our results provide strong and temporally consistent evidence of southern African monsoon strengthening in response to the deglacial and glacial meltwater-induced weakening of AMOC and subsequent North Atlantic surface cooling and associated large-scale changes in atmospheric circulations which is discussed in the following section.

5.1.3. Comparison of simulation and proxy data

We use the results of a climate simulation of Weldeab et al. (2016) to better understand the atmospheric circulation changes and seasonality of precipitation increase over the study area during HE1 and the YD. The transient simulation data were generated using LOVECLIM, a fully coupled climate model of intermediate complexity (Goosse et al., 2010). The control run includes solar insolation and greenhouse gas forcings and the extent of the Northern Hemisphere ice sheet. Freshwater forcing is applied to the North Atlantic region 50°N – 70°N to mimic AMOC changes during the HE1–Bølling–Allerød (BA)–YD transition (for more details see supplemental information). In response to the freshwater forcings, the simulated AMOC decreased significantly (Figs. 6A and B) and, as a consequence, the heat export to the North Atlantic was reduced and North Atlantic sea surface water cooled substantially (Fig. S5). The latter triggered large-scale atmospheric circulation changes that led to a southward shift and intensification of austral summer precipitation over the Indian Ocean domain, including over the study area (Fig. 7). During the austral winter, the freshwater forcing results in a moderate increase of the modeled precipitation over the study area while precipitation over eastern Africa and the western Indian Ocean (west of $\sim 75^\circ\text{E}$ and north of $\sim 7^\circ\text{S}$) is reduced relative to the results of the control run. The mean wind field during the austral winter reveals an Indian Ocean Dipole-like zonal wind pattern (Fig. 7). The austral winter wind field anomalies (relative to the control run) indicate a weakening of the wind field that drives the Indian Ocean gyre (Figure S6). With a lag of about nine months, weakening of the gyre weakens the strength of the South Equatorial Current and the Mozambique Channel throughflow (Ridderinkhof et al., 2010). As discussed in section 5.2, proxy evidence and results of the simulation indicate a weakening of the Mozambique Channel throughflow during HE1 and YD. In qualitative agreement with the proxy data, the freshwater forced simulation results suggest relatively wet conditions over our study area during the YD and HE1 compared to the control run (Figs. 6 and 7). Compared to the austral summer precipitation which shows an intensification relative to the control run (Fig. 7), the simulated precipitation increase during the austral winter is weaker (Fig. 6) and is most likely associated with a southward shift of the ITCZ during Northern Hemisphere monsoon season (austral winter). The modeled precipitation increase during austral summer

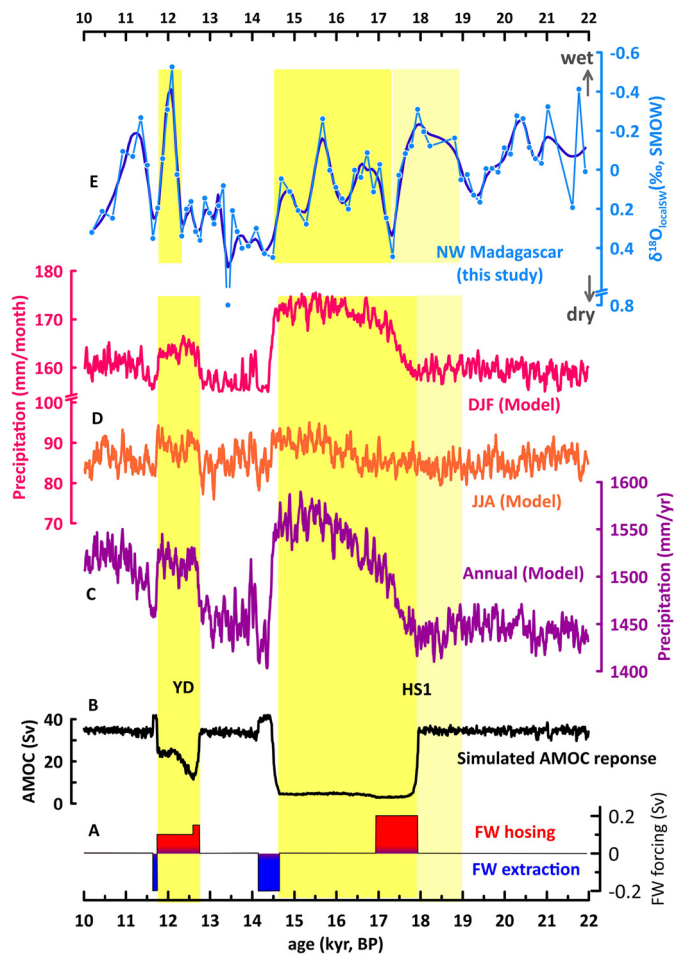


Fig. 6. Comparison of simulation- (Weldeab et al., 2016) and proxy-based hydroclimate reconstruction for northwestern Madagascar. A) Amount, timing, and duration of freshwater (FW) hosing during Heinrich event1 and YD and B) simulated response of AMOC to freshwater forcings (Weldeab et al., 2016). The effect of freshwater forcings (red) is terminated by freshwater extraction (blue). C) A 10-year average of simulated annual precipitation (mm/year) east of northern Madagascar (13.8448°S/50.625°E). D) A 10-year average of simulated monthly precipitation (mm/month) during austral summer (DJF, pink) and austral winter (JJA, orange), location as C. E) $\delta^{18}\text{O}_{\text{sw}}$ time-series analyzed in marine sediment core GIK16163-2 with a fitting curve using LOESS function shown. Yellow shaded areas indicate episodes (YD and HS1) of meltwater-induced perturbation of atmospheric and ocean circulations. The combined area shaded with dark and light yellow indicates the timing and duration of HS1, as defined by Stanford et al. (2011).

largely determines the total amount and timing of the annual precipitation increase, especially during HE1 (Figs. 6B–D).

In contrast to the proxy-based record (Fig. 6), the model results suggest a stronger precipitation increase during HS1 compared to the YD. The difference can possibly be explained by one, or a combination of the two scenarios. In addition to isotope changes due to a precipitation amount increase, the $\delta^{18}\text{O}_{\text{sw}}$ record may harbor an imprint of isotope composition changes in precipitation which can be affected by changes in the moisture source and seasonality. More likely, the model overestimated the precipitation increase during HE1 due to the arbitrarily chosen freshwater amount of the hosing experiment. We note that the trend and relative amount of the modeled last glacial precipitation deviate from the proxy evidence. Taken together, our proxy record, largely supported by the climate simulation results, provides strong and consistent evidence for southern African monsoon intensification in response to meltwater-induced perturbation of atmospheric circulation during the last deglaciation (YD and HS1) and the last glacial (HS2 and HS-like event).

5.1.4. Regional and hemispheric hydroclimate contexts

The orbital scale hydroclimate trend follows the trend of austral summer (DJF) solar insolation over the study region, though the amplitude of the $\delta^{18}\text{O}$ -sw during the mid-late Holocene is weaker compared to the $\delta^{18}\text{O}$ -sw signature of the glacial (Fig. 8A). The orbital scale hydroclimate trend is broadly consistent with the hydroclimate records of the Zambezi basin (Figs. 8D–F) (Schefuß et al., 2011; Wang et al., 2013a; Weldeab et al., 2014). In contrast to our findings, dry glacial conditions are suggested for central Madagascar based on proxy analysis in a sediment core from Lake Tritrivakely that is located at an elevation of 1778 m (Figs. 1 and 8) (Williamson et al., 1998). Similarly, relatively dry conditions during the last glacial are indicated in southwestern Madagascar (Scroxton et al., 2019) which is outside the core region of the modern southern African monsoon domain (Figs. 1 and 8). The temporal and spatial comparison of glacial hydroclimate conditions reveals a north-south gradient and an altitudinal difference, with northern Madagascar being relatively humid and central and southwestern Madagascar being relatively dry (Figs. 1 and 8), though whether the record from central Madagascar is also representative of the low elevation area remains to be confirmed. Our record of northwestern Madagascar captures glacial hydroclimate imprints that are in line with records of the Southern Hemisphere monsoon system (Cheng et al., 2012; Novello et al., 2017). Consistent with the monsoon hypothesis (Kutzbach et al., 2008), the local $\delta^{18}\text{O}_{\text{sw}}$ record during the glacial, deglacial and mid-late Holocene parallels changes in local austral summer insolation (Fig. 8A), indicating strengthening and latitudinal displacement of the ITCZ as the most likely cause for the relatively humid glacial.

On the millennial-to-centennial scale, comparison of our results with other records from central and southeastern Madagascar (Figs. 8A–F) reveals that the hydroclimate of Madagascar was temporally and spatially varied. Northwestern Madagascar that is part of the core region of the Southern Hemisphere monsoon in the African sector (Fig. 1B) experienced relatively humid conditions during the YD, HS1, H2, and the HS-like event compared with the rest of the deglaciation and the Holocene period. The lake record from central Madagascar (Fig. 8B) indicates dry conditions during the YD episode and wet conditions during HS1 and HS2 (note that here HS2 and the HS-like event are not resolved from each other) (Williamson et al., 1998), showing a mixed response to the deglacial and glacial meltwater forcings. In contrast, the speleothem record from southwestern tip of Madagascar indicates dry conditions during both YD and HS1 relative to the Bølling-Allerød and the last glacial maximum, respectively (Fig. 8F) (Scroxton et al., 2019). Paleohydroclimate studies of the Zambezi Basin show results that are partly inconsistent, despite applying the same proxy, focusing on the same basin and using marine sediment cores that were recovered from very close locations (Figs. 8D and 8E). The hydrogen isotope time-series analyzed in leaf wax indicates humid conditions in the Zambezi basin during the YD and HS1 episodes relative to the Bølling-Allerød and early Holocene (Fig. 8C) (Schefuß et al., 2011). In contrast, the same proxy as in Fig. 8C but corrected for global ice volume changes indicates no outstanding hydroclimate response to the deglacial and glacial freshwater forcings (Fig. 8D) (Wang et al., 2013a). A Ba/Ca record analyzed in *G. ruber* and applied as a proxy for runoff of the Zambezi River indicates a reduced runoff during the YD relative to the early Holocene and the Bølling-Allerød (Fig. 8E) (Weldeab et al., 2014). Furthermore, the Ba/Ca record suggests drier conditions during the late phase of HS1 relative to the Bølling-Allerød and the early part of HS1, an observation that appears to be consistent with the ice volume-corrected hydrogen isotope record (Fig. 8D) (Wang et al., 2013a), though the latter is relatively low resolved. Taken together, previous hydroclimate records draw a complex spatio-temporal pattern of millennial-scale past hydroclimate conditions

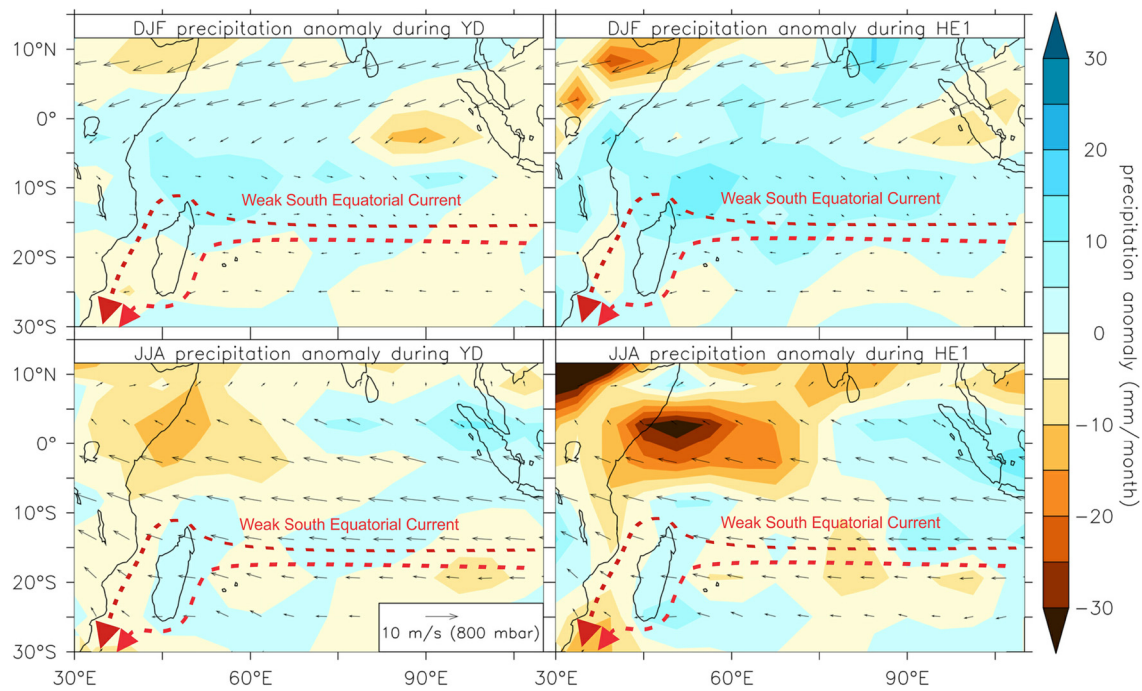


Fig. 7. Results of climate (LOVECLIM) simulation (Weldeab et al., 2016), showing seasonal precipitation and wind field changes in response to freshwater forcings. Austral summer (top) and austral winter (bottom) precipitation anomaly relative to the control run during YD (left panel) and HE1 (right panel); Black arrows indicate freshwater experiment results of direction and strength of winds at 800 mbar during YD and HE1. Red lines and arrows indicate interpretative surface currents.

of southeastern Africa. The results of our study stand out by revealing a temporally consistent hydroclimate response of the southern African monsoon. Our results add strongly to the growing consensus that the Southern Hemisphere monsoon systems strengthened and Northern Hemisphere monsoon systems weakened (Fig. 9) in response to the deglacial and glacial freshwater-induced AMOC weakening and attendant atmospheric circulation changes that include strengthening of the austral summer precipitation, as suggested by the result of climate simulation (Fig. 7).

5.2. SST gradient changes within the Mozambique Channel and weakening of Agulhas leakage

The long-term trend of our mixed layer temperature reconstruction shows a gradual increase by 2.5–3 °C between the early deglacial (18 kyr BP) and the middle Holocene (4 kyr BP) (Fig. 4). The temperature trend during the glacial and deglaciation largely parallels the trend of atmospheric CO₂ and air temperature over Antarctica (Fig. 10). With a gradual increase between the early and mid-Holocene and a decline between the mid and late Holocene by about one degree, the Holocene mixed layer temperature most likely indicates a signature of regional and global forcings. The east-west gradient of mixed layer temperature within the Mozambique Channel is largely controlled by wind fields and the wind-driven South Equatorial Current of the tropical Indian Ocean that drives Mozambique Channel throughflow (Backeberg et al., 2012). The latter propagates along the African continental margin and contributes to the manifestation of lower SSTs than in the western Mozambique Channel. Hence, we hypothesize that past spatial variation of mixed layer temperature within the Mozambique Channel provides valuable insights into changes in wind-driven water mass transport through the channel.

We use the Mg/Ca-based SST record of the western Mozambique Channel (Wang et al., 2013b) and our Mg/Ca-based composite SST record of the eastern Mozambique Channel to create a time-series of west-east SST gradient estimates (Fig. 10). Both the western and eastern Mozambique Channel Mg/Ca time-series

were analyzed in the same species and converted to temperature estimates using the same approach. Given the relatively large uncertainty of Mg/Ca-based SST reconstruction ($1\sigma: \pm 0.65^\circ\text{C}$), our focus is on long-term trends and average values over extended intervals. The SST gradient during the Holocene (0–10.5 kyr BP) shows a negative gradient with an average value of about -1°C , indicating that the current thermal gradient between the eastern and western Mozambique Channel was established since the early Holocene. During the last glacial period, the temperature gradient was negative and more variable and, on average, weaker compared to that of the mid-late Holocene. The most outstanding feature of the spatio-temporal temperature reconstruction is a gradient reversal between 15 and 18 kyr BP, indicating warmer surface water in the western Mozambique Channel as compared to the eastern Mozambique Channel water. The timing and duration of the temperature gradient reversal coincide, within age model uncertainties, with the timing of the meltwater-induced AMOC weakening during HE1, increase of atmospheric CO₂ concentration, warming of tropical oceans and air temperature rise over Antarctica (Figs. 10A–H).

A closer look reveals that the onset and duration of the gradient reversal is largely driven by an abrupt warming of the western Mozambique Channel surface water (Fig. 10F). Similar to the eastern Mozambique Channel record, surface warming of the southwestern sector of the Indian Ocean is characterized by a gradual deglacial warming (Simon et al., 2013), indicating that surface water warming in the western Mozambique Channel is not associated with changes in regions south of the Channel. We posit that this fundamental change in the thermal structure of the Mozambique Channel is linked to large-scale changes in the wind fields over the tropical Indian Ocean and, as a result, the Mozambique Channel throughflow. The latter influences the heat and salt exchanges between the tropical Indian Ocean and the Atlantic. Our association of wind field and temperature gradient changes in the Mozambique Channel is consistent with two key and interrelated results of the hosing experiment. Relative to the modern conditions (Fig. 1), the hosing experiment results indicate a weakening of the

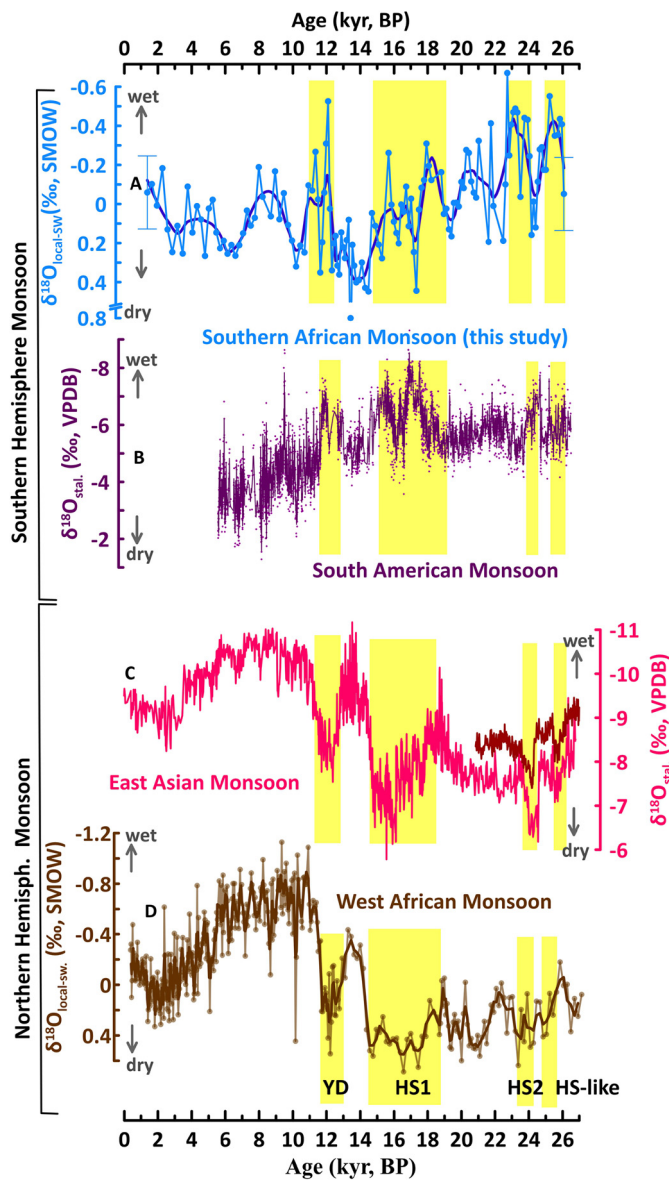


Fig. 9. Millennial-scale meltwater-induced climate changes (yellow shaded intervals) and associated response of Northern Hemisphere and Southern Hemisphere monsoon systems. A) $\delta^{18}O_{sw}$ of core GIK16163-2 (this study) with a fitting curve using LOESS function. B) $\delta^{18}O$ of stalagmites from Jaragua Cave in Brazil (Novello et al., 2017) as a proxy for South American monsoon changes. C) $\delta^{18}O$ of stalagmites from Dongge Cave and Wulu Cave in China (Cheng et al., 2012; Zhao et al., 2010) as proxy of East Asian monsoon. D) Reconstruction of West African monsoon based on changes temperature and ice volume-corrected $\delta^{18}O$ composition of local mixed layer water calculated from $\delta^{18}O$ analyzed in *G. ruber* in a Gulf of Guinea sediment core (Weldeab et al., 2007).

16.7±3.1 Sv and falls within the upper range of observed variability (Ridderinkhof et al., 2010).

Noting that, based on current observations, the Agulhas leakage is controlled by the latitude of maximum (Southern Hemisphere) westerlies and strength of wind fields over the Indian Ocean (Backeberg et al., 2012; Beal and Elipot, 2016; Biastoch et al., 2015), we hypothesize that the reduced Mozambique Channel throughflow weakened the Agulhas Current and Agulhas leakage during HS1.

Previous studies, based on records mostly from sites off southern Africa, suggest a strengthening of Agulhas leakage during deglaciations (Caley et al., 2012; Franzese et al., 2009; Peeters et al., 2004; Simon et al., 2013). A close look at the millennial-scale segments of the records, though complicated by the low resolu-

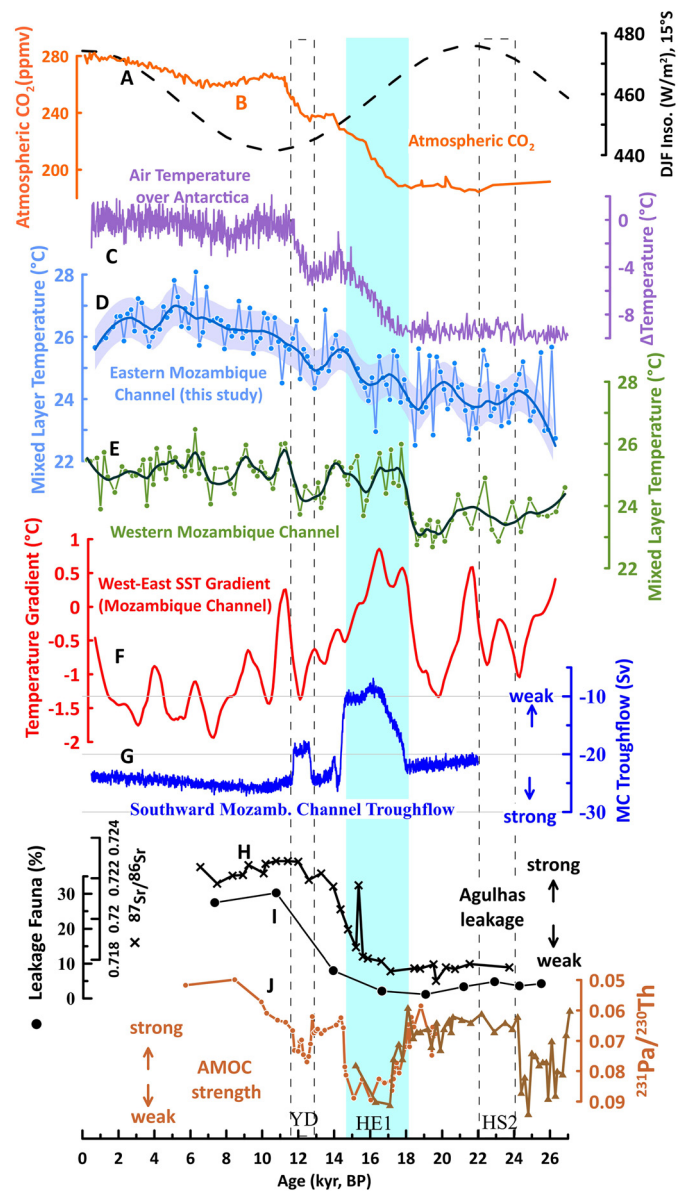


Fig. 10. Mixed layer temperature gradient changes within the Mozambique Channel and its potential association with a weak Mozambique Channel throughflow and weak Agulhas leakages. A) Austral summer solar insolation at 15° S (Laskar et al., 2004). B) Atmospheric CO₂ concentration analyzed in Antarctica ice cores (Luthi et al., 2008). C) Changes in air temperature over Antarctica (Dome C) relative to the year 1950 (Jouzel et al., 2007). D) Mg/Ca-based composite mixed layer temperature record in eastern Mozambique Channel (this study) and (E) in western Mozambique Channel (Wang et al., 2013b). F) West-east SST gradient within Mozambique Channel calculated using temperature time-series shown in Fig. 10D and 10E. G) Model-based estimates of southward Mozambique throughflow (this study). Negative values indicate southward direction of the water mass transport. For the freshwater amount and duration of the hosing experiment during HE1 and YD see Fig. 6A. H. I) Agulhas leakage fauna in percentage (Peeters et al., 2004) and Strontium isotope ratios analyzed in terrigenous components of marine sediments from the Cape Basin (Franzese et al., 2009) and used as a proxy for the strength of Agulhas leakage. J) $^{231}Pa/^{230}Th$ analyzed in North Atlantic sediment cores and used as a proxy for relative changes in AMOC (Lippold et al., 2009; McManus et al., 2004). Blue shaded area indicates the time period of positive west-east SST gradient.

tion of the time-series, reveals that during Heinrich stadials the Agulhas leakage proxy draws a complex and temporally variable picture, with some Heinrich episodes accompanied by a reduced Agulhas leakage and others by an increased Agulhas leakage (Simon et al., 2013). It should be noted that reconstruction sites within the Indian Ocean sector of the Agulhas Current may also harbor signatures of Agulhas Return Current (Simon et al., 2013).

Hence, we compare our results with the record of Peeters et al. (2004) that focuses on marine sediments from the Cape Basin (Atlantic sector, west of the retroflexion and within the shedding region) that is most likely to capture changes in the Agulhas leakage. The foraminiferal assemblage-based reconstruction (Peeters et al., 2004) indicates a reduced Agulhas leakage during HE1, though the resolution is relatively low (Fig. 10I). Consistent with the faunal assemblage, a reduced terrigenous sediment deposition from the southeastern African continental margins in the Cape Basin suggests a weak glacial and deglacial Agulhas leakage (Franzese et al., 2009). Satellite data and modeling studies reveal that due to the current warming climate the Subtropical Front and the latitude of maximum westerlies are shifting southward, allowing enhanced Agulhas leakage (Backeberg et al., 2012; Biastoch et al., 2015). Similarly, parallel to the rise of air temperature over Antarctica, warming of the Southern Ocean, and atmospheric CO₂ concentration increase (Fig. 10B), proxy-based reconstructions suggest a southward shift of the Subtropical Front and the Southern Hemisphere westerlies during HE1 (Anderson et al., 2009). A weakened Agulhas leakage at the time of southward shifted westerlies is inconsistent with the notion of a position shift of the westerlies as the most dominant factor that controls Agulhas leakage. In fact, as detailed in Beal and Elipot (2016), modern observations indicate that a complex interplay and non-linear dynamics between shift of the latitude of maximum westerlies and the strength of Agulhas Current modulates the Agulhas leakage. We hypothesize that weakening of the tropical Indian Ocean gyre and, as a result, Southern Equatorial Currents during HE1 weakened the Agulhas Current and reduced the Agulhas leakage or maintained at its last glacial maximum level, though for the latter a combination of a northerly position of the westerlies (Peeters et al., 2004) and weak Agulhas Current (Franzese et al., 2009) have been invoked. The broader implication that emerges from our study is that the changes in the tropical Indian Ocean wind fields in response to meltwater-induced perturbation of atmospheric circulations created a feedback that could have contributed to sustaining the weakened AMOC during Heinrich events by reducing the amount of salt leakage into the Atlantic.

6. Summary and conclusion

Our study indicates that the core region of southern African monsoon was relatively humid during the last glacial and during YD, HS1, HS2, and HS-like event prior to HS2. Our findings add to the growing consensus that the Southern Hemisphere monsoon systems are highly sensitive to meltwater inputs into the North Atlantic and the ensuing perturbation of ocean and atmospheric circulations.

Comparison of sea surface temperature records within the Mozambique Channel reveals a reversal of the west-east gradient during HE1. The reversal indicates a fundamental thermal reorganization associated with a weakening of the wind-driven Southern Equatorial Current and, as a result, a weakening of Mozambique Channel throughflow that constitutes a significant component of salty water masses that feed the Agulhas Current. The strength of the Agulhas Current modulates the variability of Agulhas leakage that is thought to affect AMOC variability. The weakening of the Southern Equatorial Current and Mozambique Channel throughflow in response to meltwater-induced perturbations of northern high latitude climate potentially presents a feedback mechanism that might have contributed to sustaining a weakened AMOC during Heinrich stadials by reducing the Agulhas leakage.

CRediT authorship contribution statement

Weldeab designed the concept of the study. Ma prepared the samples for radiocarbon, trace element, stable isotope analyses, analyzed the data and performed the data visualization. Ma and Weldeab wrote the draft of the manuscripts. Schneider designed and led the marine sediment collection campaign. Schneider, Weldeab, and Andersen collected the sediment cores. Garbe-Schönberg and Andersen carried out the trace element and isotope analyses, respectively. Friedrich conducted and analyzed the climate simulations. All authors have discussed and contributed to the final version of the manuscript.

Declaration of competing interest

The authors declare that they have no known competing financial interests or personal relationships that could have appeared to influence the work reported in this paper.

Acknowledgements

We thank Dr. Dorothy K. Pak for discussion, Dr. Mattias Hüls for radiocarbon measurements, Dipl.-Ing. Ulrike Westernströer for help with ICP-SFMS analyses, the two reviewers for their constructive comments and suggestions that improved the previous version of the manuscript and Dr. Yemane Asmerom, the Editor, for his handling of the paper. The data presented in this study are available at www.pangaea.de.

Appendix A. Supplementary material

Supplementary material related to this article can be found online at <https://doi.org/10.1016/j.epsl.2021.117148>.

References

- Alley, R.B., 2000. The Younger Dryas cold interval as viewed from central Greenland. *Quat. Sci. Rev.* 19, 213–226.
- Anderson, R.F., Ali, S., Bradtmiller, L.I., Nielsen, S.H.H., Fleisher, M.Q., Anderson, B.E., Burckle, L.H., 2009. Wind-driven upwelling in the Southern Ocean and the deglacial rise in atmospheric CO₂. *Science* 323, 1443–1448.
- Backeberg, B.C., Penven, P., Rouault, M., 2012. Impact of intensified Indian Ocean winds on mesoscale variability in the Agulhas system. *Nat. Clim. Change* 2, 608–612.
- Beal, L.M., Elipot, S., 2016. Broadening not strengthening of the Agulhas Current since the early 1990s. *Nature* 540, 570–573.
- Behringer, D.W., Xue, Y., 2004. Evaluation of the global ocean data assimilation system at NCEP: the Pacific Ocean. In: Eighth Symposium on Integrated Observing and Assimilation Systems for Atmosphere, Oceans, and Land Surface AMS 84th Annual Meeting. Washington State Convention and Trade Center, Seattle, Washington, pp. 11–15.
- Biastoch, A., Durgadoo, J.V., Morrison, A.K., van Sebille, E., Weijer, W., Griffies, S.M., 2015. Atlantic multi-decadal oscillation covaries with Agulhas leakage. *Nat. Commun.* 6. <https://doi.org/10.1038/ncomms10082>.
- Blaauw, M., Christen, J.A., 2011. Flexible paleoclimate age-depth models using an autoregressive gamma process. *Bayesian Anal.* 6, 457–474.
- Bond, G., Showers, W., Cheseby, M., Lotti, R., Almasi, P., deMenocal, P., Priore, P., Cullen, H., Hajdas, I., Bonani, G., 1997. A pervasive millennial-scale cycle in north Atlantic Holocene and glacial climates. *Science* 278, 1257–1266.
- Bowen, G.J., Revenaugh, J., 2003. Interpolating the isotopic composition of modern meteoric precipitation. *Water Resour. Res.* 39. <https://doi.org/10.1029/2003WR002086>.
- Caley, T., Giraudeau, J., Malaize, B., Rossignol, L., Pierre, C., 2012. Agulhas leakage as a key process in the modes of Quaternary climate changes. *Proc. Natl. Acad. Sci.* 109, 6835–6839.
- Cheng, H., Sinha, A., Wang, X., Cruz, F., Edwards, R., 2012. The Global Paleomonsoon as seen through speleothem records from Asia and the Americas. *Clim. Dyn.* 39, 1045–1062.
- Franzese, A.M., Hemming, S.R., Goldstein, S.L., 2009. Use of strontium isotopes in detrital sediments to constrain the glacial position of the Agulhas Retroflexion. *Paleoceanography* 24, PA2217.

- Goosse, H., Brovkin, V., Fichefet, T., Haarsma, R., Huybrechts, P., Jongma, J., Mouchet, A., Selten, F., Barriat, P.Y., Campin, J.M., Deleersnijder, E., Driesschaert, E., Goelzer, H., Janssens, I., Loutre, M.F., Maqueda, M.A.M., Opsteegh, T., Mathieu, P.P., Munhoven, G., Pettersson, E.J., Renssen, H., Roche, D.M., Schaeffer, M., Tartinville, B., Timmermann, A., Weber, S.L., 2010. Description of the Earth system model of intermediate complexity LOVECLIM version 1.2. *Geosci. Model Dev.* 3, 603–633.
- Huffman, G.J., Stocker, E.F., Bolvin, D.T., Nelkin, E.J., Tan, J., 2019. GPM IMERG Final Precipitation L3 1 month 0.1 degree x 0.1 degree V05, Greenbelt, MD. Goddard Earth Sciences Data and Information Services Center (GES DISC). <https://doi.org/10.5067/GPM/IMERG/3B-MONTH/06>. (Accessed 30 October 2020).
- Hutchinson, K., Beal, L.M., Penven, P., Anson, I., Hermes, J., 2018. Seasonal phasing of Agulhas Current transport tied to a baroclinic adjustment of near-field winds. *J. Geophys. Res.*, *Oceans* 123, 7067–7083.
- Jouzel, J., Masson-Delmotte, V., Cattani, O., Dreyfus, G., Falourd, S., Hoffmann, G., Minster, B., Nouet, J., Barnola, J.M., Chappellaz, J., Fischer, H., Gallet, J.C., Johnsen, S., Leuenberger, M., Loulergue, L., Luthi, D., Oerter, H., Parrenin, F., Raisbeck, G., Raynaud, D., Schilt, A., Schwander, J., Selmo, E., Souchez, R., Spahni, R., Stauffer, B., Steffensen, J.P., Stenni, B., Stocker, T.F., Tison, J.L., Werner, M., Wolff, E.W., 2007. Orbital and millennial Antarctic climate variability over the past 800,000 years. *Science* 317, 793–796.
- Kalnay, E., Kanamitsu, M., Kistler, R., Collins, W., Deaven, D., Gandin, L., Iredell, M., Saha, S., White, G., Woollen, J., Zhu, Y., Chelliah, M., Ebisuzaki, W., Higgins, W., Janowiak, J., Mo, K.C., Ropelewski, C., Wang, J., Leetmaa, A., Reynolds, R., Jenne, R., Joseph, D., 1996. The NCEP/NCAR 40-year reanalysis project. *Bull. Am. Meteorol. Soc.* 77, 437–471.
- Khon, V.C., Wang, Y.V., Krebs-Kanzow, U., Kaplan, J.O., Schneider, R.R., Schneider, B., 2014. Climate and CO₂ effects on the vegetation of southern tropical Africa over the last 37,000 years. *Earth Planet. Sci. Lett.* 403, 407–417.
- Kutzbach, J.E., Liu, X., Liu, Z., Chen, G., 2008. Simulation of the evolutionary response of global summer monsoons to orbital forcing over the past 280,000 years. *Clim. Dyn.* 30, 567–579.
- Laskar, J., Robutel, P., Joutel, F., Gastineau, M., Correia, A.C.M., Levrard, B., 2004. A long-term numerical solution for the insolation quantities of the Earth. *Astron. Astrophys.* 428, 261–285.
- Lippold, J., Grützner, J., Winter, D., Lahaye, Y., Mangini, A., Christl, M., 2009. Does sedimentary 231Pa/230Th from the Bermuda Rise monitor past Atlantic Meridional Overturning Circulation? *Geophys. Res. Lett.* 36, L12601. <https://doi.org/10.1029/2009GL038068>.
- Lougheed, B.C., Obrochta, S.P., 2019. A rapid, deterministic age-depth modeling routine for geological sequences with inherent depth uncertainty. *Paleoceanogr. Paleoclimatol.* 34, 122–133.
- Luthi, D., Le Floch, M., Bereiter, B., Blunier, T., Barnola, J.M., Siegenthaler, U., Raynaud, D., Jouzel, J., Fischer, H., Kawamura, K., Stocker, T.F., 2008. High-resolution carbon dioxide concentration record 650,000–800,000 years before present. *Nature* 453, 379–382.
- Malauene, B.S., Shillington, F.A., Roberts, M.J., Moloney, C.L., 2014. Cool, elevated chlorophyll-a waters off northern Mozambique. *Deep-Sea Res., Part 2, Top. Stud. Oceanogr.* 100, 68–78.
- Marino, G., Zahn, R., Ziegler, M., Purcell, C., Knorr, G., Hall, I.R., Ziveri, P., Elderfield, H., 2013. Agulhas salt-leakage oscillations during abrupt climate changes of the Late Pleistocene. *Paleoceanography* 28, 599–606.
- Martrat, B., Grimalt, J.O., Shackleton, N.J., de Abreu, L., Hutterli, M.A., Stocker, T.F., 2007. Four climate cycles of recurring deep and surface water destabilizations on the Iberian margin. *Science* 317, 502–507.
- Mayewski, P.A., Meeker, L.D., Twickler, M.S., Whitlow, S., Yang, Q., Lyons, W.B., Prentice, M., 1997. Major features and forcing of high-latitude northern hemisphere atmospheric circulation using a 110,000-year-long glaciochemical series. *J. Geophys. Res.*, *Oceans* 102, 26345–26366.
- McManus, J.F., Francois, R., Gherardi, J.-M., Keigwin, L.D., Brown-Leger, S., 2004. Collapse and rapid resumption of Atlantic meridional circulation linked to deglacial climate changes. *Nature* 428, 834–837.
- Novello, V.F., Cruz, F.W., Vuille, M., Strikis, N.M., Edwards, R.L., Cheng, H., Emerick, S., de Paula, M.S., Li, X., Barreto, E.S., Karmann, I., Santos, R.V., 2017. A high-resolution history of the South American Monsoon from Last Glacial Maximum to the Holocene. *Sci. Rep.* 7, 44267.
- Peeters, F.J.C., Acheson, R., Brummer, G.J.A., de Ruijter, W.P.M., Schneider, R.R., Ganssen, G.M., Ufkes, E., Kroon, D., 2004. Vigorous exchange between the Indian and Atlantic oceans at the end of the past five glacial periods. *Nature* 430, 661–665.
- Ridderinkhof, H., van der Werf, P.M., Ullgren, J.E., van Aken, H.M., van Leeuwen, P.J., de Ruijter, W.P.M., 2010. Seasonal and interannual variability in the Mozambique Channel from moored current observations. *J. Geophys. Res.* 115, C06010.
- Saji, N.H., Goswami, B.N., Vinayachandran, P.N., Yamagata, T., 1999. A dipole mode in the Indian Ocean. *Nature* 401, 360–363.
- Schefuß, E., Kuhlmann, H., Mollenhauer, G., Prange, M., Patzold, J., 2011. Forcing of wet phases in southeast Africa over the past 17,000 years. *Nature* 480, 509–512.
- Scroton, N., Burns, S.J., McGee, D., Hardt, B., Godfrey, L.R., Ranivoharimanana, L., Faina, P., 2019. Competing temperature and atmospheric circulation effects on southwest Madagascar rainfall during the last deglaciation. *Paleoceanogr. Paleoclimatol.* 34, 275–286.
- Simon, M.H., Arthur, K.L., Hall, I.R., Peeters, F.J.C., Loveday, B.R., Barker, S., Ziegler, M., Zahn, R., 2013. Millennial-scale Agulhas Current variability and its implications for salt-leakage through the Indian–Atlantic Ocean Gateway. *Earth Planet. Sci. Lett.* 383, 101–112.
- Simonsen, M.F., Baccolo, G., Blunier, T., Borunda, A., Delmonte, B., Frei, R., Goldstein, S., Grinsted, A., Kjær, H.A., Sowers, T., Svensson, A., Vinther, B., Vladimirova, D., Winckler, G., Winstrup, M., Vallelonga, P., 2019. East Greenland ice core dust record reveals timing of Greenland ice sheet advance and retreat. *Nat. Commun.* 10. <https://doi.org/10.1038/s41467-019-12546-41462>.
- Stanford, J.D., Rohling, E.J., Bacon, S., Roberts, A.P., Grousset, F.E., Bolshaw, M., 2011. A new concept for the paleoceanographic evolution of Heinrich event 1 in the North Atlantic. *Quat. Sci. Rev.* 30, 1047–1066.
- Swart, N.C., Lutjeharms, J.R.E., Ridderinkhof, H., de Ruijter, W.P.M., 2010. Observed characteristics of Mozambique Channel eddies. *J. Geophys. Res.* 115. <https://doi.org/10.1029/2009jc005875>.
- U.S. Geological Survey's Center for Earth Resources Observation and Science, E., 1996. 30 arc-second DEM of Africa. <https://doi.org/10.5067/F7DF6PQS>.
- Voarintsoa, N.R.G., Railsback, L.B., Brook, G.A., Wang, L.X., Kathayat, G., Cheng, H., Li, X.L., Edwards, R.L., Rakotondrazafy, A.F.M., Razanatsheho, M.O.M., 2017. Three distinct Holocene intervals of stalagmite deposition and nondeposition revealed in NW Madagascar, and their paleoclimate implications. *Clim. Past* 13, 1771–1790.
- Wang, Y.V., Larsen, T., Leduc, G., Andersen, N., Blanz, T., Schneider, R.R., 2013a. What does leaf wax δD from a mixed C3/C4 vegetation region tell us? *Geochim. Cosmochim. Acta* 111, 128–139.
- Wang, Y.V., Leduc, G., Regenberg, M., Andersen, N., Larsen, T., Blanz, T., Schneider, R.R., 2013b. Northern and southern hemisphere controls on seasonal sea surface temperatures in the Indian Ocean during the last deglaciation. *Paleoceanography*. <https://doi.org/10.1002/palo.20053>.
- Weldeab, S., 2012. Bipolar modulation of millennial-scale West African monsoon variability during the last glacial (75,000–25,000 years ago). *Quat. Sci. Rev.* 40, 21–29.
- Weldeab, S., Friedrich, T., Timmermann, A., Schneider, R.R., 2016. Strong middepth warming and weak radiocarbon imprints in the equatorial Atlantic during Heinrich 1 and Younger Dryas. *Paleoceanography* 31, 1070–1082.
- Weldeab, S., Lea, D.W., Oberhänsli, H., Schneider, R.R., 2014. Links between southwestern tropical Indian Ocean SST and precipitation over southeastern Africa over the last 17kyr. *Palaeogeogr. Palaeoclimatol. Palaeoecol.* 410, 200–212.
- Weldeab, S., Lea, D.W., Schneider, R.R., Andersen, N., 2007. 155,000 years of West African monsoon and ocean thermal evolution. *Science* 316, 1303–1307.
- Wentz, F., Yueh, S., Lagerloef, G., 2014. Aquarius Level 3 Sea Surface Salinity Standard Mapped Image Annual Data V3.0. Ver. 3.0. PO.DAAC, CA, USA. <https://doi.org/10.5067/AQUAR-3SAPS>. (Accessed 30 October 2020).
- Williamson, D., Jelinowska, A., Kissel, C., Tucholka, P., Gibert, E., Gasse, F., Massault, M., Taieb, M., Van Campo, E., Wieckowski, K., 1998. Mineral-magnetic proxies of erosion/oxidation cycles in tropical maar-lake sediments (Lake Tritrivakely, Madagascar): paleoenvironmental implications. *Earth Planet. Sci. Lett.* 155, 205–219.
- Zhao, K., Wang, Y., Edwards, R.L., Cheng, H., Liu, D., 2010. High-resolution stalagmite $\delta^{18}O$ records of Asian monsoon changes in central and southern China spanning the MIS 3/2 transition. *Earth Planet. Sci. Lett.* 298, 191–198.